



# Modelling of an expandable, reconfigurable, renewable DC microgrid for off-grid communities

J. Kitson <sup>a</sup>, S.J. Williamson <sup>a,\*</sup>, P.W. Harper <sup>a</sup>, C.A. McMahon <sup>b</sup>, G. Rosenberg <sup>a</sup>, M.J. Tierney <sup>a</sup>, K. Bell <sup>c</sup>, B. Gautam <sup>d</sup>

<sup>a</sup> Faculty of Engineering, University of Bristol, University Walk, Bristol, UK

<sup>b</sup> DTU Technical University of Denmark, Lyngby, Denmark

<sup>c</sup> School for Policy Studies, University of Bristol, Bristol, UK

<sup>d</sup> People, Energy & Environmental Development Association (PEEDA), Kathmandu, Nepal

## ARTICLE INFO

### Article history:

Received 19 December 2017

Received in revised form

26 June 2018

Accepted 29 June 2018

Available online 30 June 2018

### Keywords:

DC microgrid

DC non-linear droop control

Solar

Wind

## ABSTRACT

This paper proposes a DC microgrid system, comprising multiple locally available renewable energy sources in an off-grid rural community, based on a commissioned field study carried out in a rural, off-grid village in Nepal, which has solar and wind resource available. Using estimated solar data for the site's location, wind data measured locally, household and population data collected over the course of several months and typical measured domestic demand profiles, DC microgrid system models have been constructed using HOMER and Simulink software to represent the DC system proposed.

This work is innovative in using a range of on-site data collected and measured locally in a commissioned field study carried out over several months to quantify current local resources and loads and estimating future ones based on the local population's current economic and domestic activities, and intended ones. This data is used in determining both the optimal size of the generation and storage elements through HOMER based on long term system behaviour, and to model shorter term system response to changes in generation and load using Simulink, ensuring system stability and grid voltage is maintained. Further novel aspects of this study are that power flow is controlled using adaptive DC droop control on each individual energy source to enable optimal power sharing with minimum power dissipation across distribution lines, and the droop control has been further adapted to the case of storage which can act as a source or a load.

© 2018 Elsevier Ltd. All rights reserved.

## 1. Introduction

Of the 1.2 billion people who do not have access to electricity, nearly 85% are in rural areas [1], and most of these will require off-grid solutions to achieve the U.N.'s goal of universal energy access by 2030 [2]. For these solutions, renewable generation technologies are often the most appropriate, as they are sustainable and allow local power generation without any requirement for external energy supply. Off-grid renewable solutions are normally on an individual household scale, such as the Solar-Home System (SHS), or community scale solutions, where a single resource powers multiple households such as a micro-hydro scheme. Microgrids have

emerged as an opportunity to connect multiple sources and loads that are in close geographic proximity, and can be either grid-connected or islanded.

Both AC- and DC-based microgrids have been investigated [3], with benefits and drawbacks to each type of system. AC networks are often implemented, as they replicate the standard electrical distribution system, with their technology understood, able to change voltage levels simply to transmit longer distances, and a well-developed supply chain of end-use equipment. However, DC microgrids have advantages of simpler control with no requirement for synchronisation, and are able to integrate renewable sources such as photovoltaics and battery storage easier than AC networks, can produce systems with lower losses due to the ability to dispense with AC-DC power conversion and as such are being increasingly investigated [4,5]. Primary control for DC microgrids can be based on droop mechanisms, where the output voltage of a source reduces as the power demand increases, mimicking grid

\* Corresponding author.

E-mail addresses: [joanne.eemg.kitson@bristol.ac.uk](mailto:joanne.eemg.kitson@bristol.ac.uk) (J. Kitson), [sam.williamson@bristol.ac.uk](mailto:sam.williamson@bristol.ac.uk) (S.J. Williamson).

attributes [3]. This can be achieved artificially through power electronic interfaces so that power flow can be balanced autonomously between sources without central control, with further levels of control added as required [6]. Additional control levels can be included in the grid system, to support maintaining voltage and frequency of the grid, coordinating the actions of several generation, storage and load units within the system [3,7].

There are many different software packages that can be used to evaluate hybridised energy, with the National Renewable Energy Laboratory's Hybrid Optimisation Model for Electric Renewables (HOMER) being the most popular for whole energy system analysis [8]. HOMER is a whole energy system modelling tool, with an economic analyser to optimise and assess the financial viability of a system design. However, the number of inputs in hybrid system is limited within the software, and it is unable to model the system at a detailed level to evaluate different control schemes or rapid load changes to evaluate rapid system response. There are many papers that design microgrid systems using HOMER, such as [9–11], developing an optimised system design based on local parameters. Studies such as [12,13] have used linear programming techniques within Matlab to develop the microgrid model and evaluate their performance in relation to the dynamic performance, requiring mathematically-derived models of each individual component within the system. More simply, Matlab's Simulink has been used by numerous studies, such as [14–16], to model control and dynamic performance of microgrid systems successfully, but without the ability to optimise the system design for overall performance or economic sustainability. Several studies have used both these two software packages, such as [17–19], using HOMER to size, optimise and evaluating the overall system performance, whilst using Simulink to control the system [17], perform a load analysis [18], or understand the complimentary nature of the different resources on the system [19]. These works however do not combine data collected from off-grid communities collected through social surveys, with system simulation at a low level, and overall system design optimisation.

Several studies have considered different control regimes and design rules for off-grid and grid-connected DC microgrids. [20] and [21] review the general themes of microgrid topology, control and protection systems, comparing AC and DC systems and their relative advantages and drawbacks, providing pilot study data and information, and concluding that standardisation, cost reduction, and optimising system management will be key to improving their future market penetration. The standardisation of control structures for microgrids has been approached by Ref. [3], to develop a more formal hierarchical control structure to allow for integration across multiple platforms. [22] discusses the design of a hybrid photovoltaic, wind and fuel cell topology that is grid-connected, managing the load by using standard proportional-integral controllers along with perturb and observe algorithms for maximum power point tracking. This DC microgrid control feeds onto a fixed bus, and exports all power onto an AC grid, and so the control involved no supply-demand management on the grid, or storage control. [23] develops a higher-level control system, using cost as a basis of generation source scheduling, and utilising a standard linear droop control to implement power sharing between sources.

This paper proposes and simulates a multi-source modular DC microgrid system in which the sources interfaced with the DC grid are managed via droop control with intended implementation in village in Nepal as a specific case study. The novelty of this work is a through the combination of real energy source and load data, population and social data with short and long-term energy modelling, to assess DC system control and proposed capacity to enable a realistic prediction of energy provision. Specifically, (1) bespoke energy source and demand data has been measured and

collected on the authors' behalf locally over the course of several months and social surveys carried out to assess site's and population's renewable resources and energy needs. (2) This measured data has informed simulations, to account for short term (at a scale of minutes and hours) for system specification and control strategies. This includes a novel adaptive DC droop control operating on individual energy sources acting as an energy source or sink, to minimise system transmission losses. Additionally, (3) longer term measurements at hourly intervals over a number of months (e.g. local wind measurements undertaken) have been used in conjunction with measured data on population, questionnaires and predicted demands, in order to model requirements for capacity and storage over the course of a year.

Section 2 describes the overall system layout and design; Section 3 details the case study site; Section 4 describes the construction of the model microgrid in Simulink for system parameters and droop control. Section 5 presents sizing analyses of the system using HOMER software, presenting and discussing the results from the case study site and demonstrating the improved site performance.

## 2. DC microgrid system overview

The DC microgrid architecture applied in this study links together sources, storage and loads in a common location; the sources, storage and loads can be scattered across the implementation area, as shown diagrammatically in Fig. 1.

As illustrated in Fig. 1, it is intended that each source or storage element is connected onto the grid through a modular power electronic interface comprising maximum power point tracking (MPPT) or charge control as a first stage and droop control as a second stage. The droop control stage on each source or storage element regulates the voltages the voltage of that source to the grid level within the permissible DC grid voltage range set out in Table 4, by using droop control to manage the power flow onto the grid.

Droop control is used to control the power flow of the system without the need for communication between sources. For DC systems, the converter measures its output power or current and adjusts the output voltage. This is typically implemented as a linear relationship [3] illustrated in Fig. 2 (a); thus, for sources that are separated by transmission and distribution lines, there is a trade-off between voltage regulation and power sharing. However, a system was proposed in Ref. [24], which uses a non-linear droop curve, shown in Fig. 2 (b). This allows for good power sharing at low and high power, whilst minimising change in grid voltage. As with a linear droop scheme, a non-linear droop control system can be scaled dependent on the ratio of available power to maximum power [25]. In this work, the non-linear droop control applied to sources in Ref. [24] has been extended and adapted for use with a

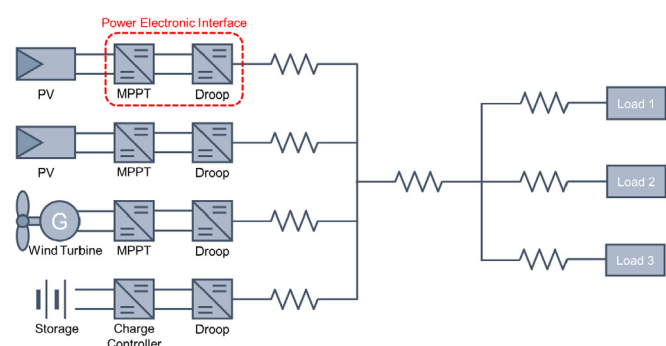


**Fig. 1.** Diagram of off-grid distributed DC multi-source, multi-load system.

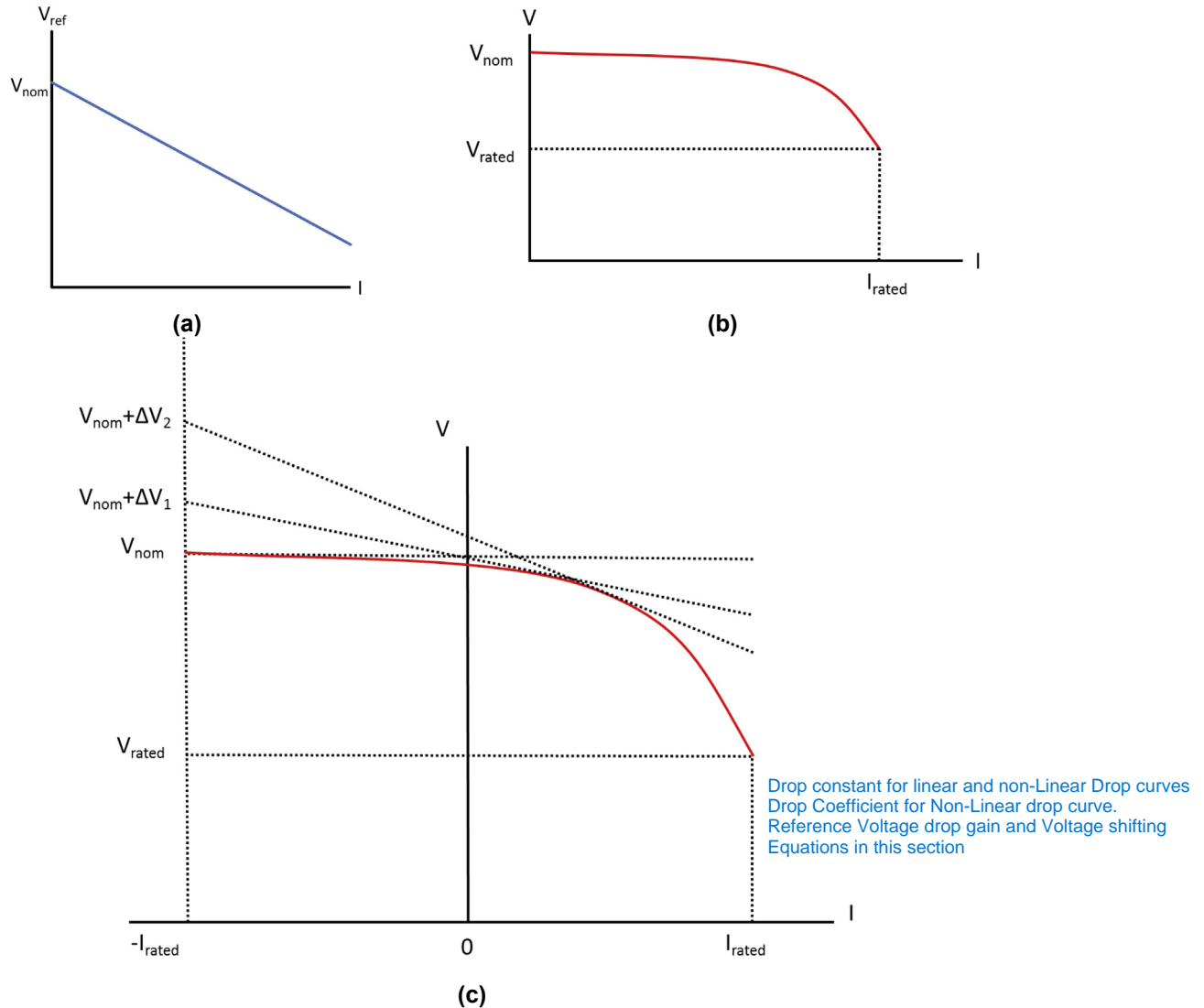


**Fig. 2.** (a) Linear and (b) non-linear droop control curves for sources, and (c) non-linear droop curve for storage elements with its mathematical derivation.

storage element. As shown in Fig. 2 (c), the droop control voltage demand is offset on the horizontal axis to allow an element that absorbs current to accommodate charging, as well as acting as a current source during discharge. This allows the storage element to recharge the storage system at times of low system load, and discharge the battery when there is high demand. As with the wind and solar sources, the droop curve for storage can be scaled as a proportion of storage state-of-charge, allowing the system to adapt to instantaneous conditions.

The droop gradient used in linear droop control is defined mathematically by the voltage regulation boundaries for a system ( $V_{NOM}$  and  $V_{RATED}$ ) and the output power or output current range from the device or source, as shown in Equation (1)

$$m = \frac{V_{RATED} - V_{NOM}}{I_{RATED}} \quad \text{Slope resistance of droop for linear} \quad (1)$$

where  $m$  is the droop gradient,  $V_{NOM}$  is the nominal (maximum) voltage in the system,  $V_{RATED}$  is the rated (minimum) voltage in the system and  $I_{RATED}$  is the rated (maximum) output current from the device. When this altered to a bi-directional system, for energy storage or grid interface, then the rated current can be either

supplied or sunk into the device, so the gradient is half the unidirectional value.

For non-linear droop control, the equations from Ref. [24] have been extended in this work to enable a storage element to act as a current source or sink. Thus, the revised equation for a reference voltage based on non-linear droop becomes Eqn. (2) where  $m$  is the arc constant and  $\alpha$  is the arc coefficient

$$V_{ref} = V_{NOM} - m(I + I_{RATED})^\alpha \quad (2)$$

The revised arc constant for source and sink non-linear regulation is expressed as in Eqn. (3).

$$m = \frac{V_{NOM} - V_{RATED}}{(2I_{RATED})^\alpha} \quad \begin{array}{l} m = \text{change in y/ change in x} \\ m = V_{nom} - V_{rated} / (I_{rated} - (-I_{rated})) \\ m = V_{nom} - V_{rated} / 2I_{rated} \end{array} \quad (3)$$

In order to calculate the droop gain ( $R_d$ ) at any point in the droop curve, this is calculated by taking the derivative of the reference voltage with respect to current, Eqn. (4).

$$R_d = \frac{\delta V_{ref}}{\delta I} = -m\alpha(I + I_{RATED})^{\alpha-1} \quad (4)$$

The droop gain can therefore be expressed in terms of rated

current and voltage as in Eqn. (5)

$$R_d = \frac{-\alpha(V_{NOM} - V_{RATED})(I + I_{RATED})^{\alpha-1}}{(2I_{RATED})^\alpha} \quad (5)$$

The equivalent voltage shifting along the axis that can be calculated by intersecting the equivalent droop line at a specific operating point with the voltage axis equivalent to  $-I_{RATED}$  can be expressed as in Eqn. (6)

$$\Delta V = \frac{(\alpha - 1)(V_{NOM} - V_{RATED})(I + I_{RATED})^\alpha}{(2I_{RATED})^\alpha} \quad (6)$$

The revised coefficient for the non-linear source and sink curve is expressed as in Eqn. (7)

$$\alpha = \frac{2R_{dmax}I_{RATED}}{V_{NOM} - V_{RATED}} \quad \text{from (5) with } a = 1 \quad (7)$$

These equations derive the curve shown in Fig. 2 (c).

The grid transmission and distribution system is constructed from wires, which can be assumed to be simple resistances for low voltage cables (up to approximately 1.5 kV). The loads for the DC microgrid are assumed to connect directly onto the grid and cannot gain any additional electrical power from other sources.

### 3. Case study site: Ruksibhanjyang village, Mityal VDC, Nepal

#### 3.1. Site information

A case study example is used to demonstrate the DC microgrid system described in Section 2. The site selected is Ruksibhanjyang, Mityal VDC, Palpa, Nepal, which is shown in Fig. 3, where a field study has been carried out by a Nepalese partner NGO called "People, Energy & Environment Development Association" (PEEDA) [26] to determine the energy needs of this community. PEEDA have been operating since 1997 and have considerable experience in assessment and practical implementation of microgrids [27]. This site was chosen as a case study because it is an off-grid community with scope for implementing both solar and wind energy sources for a combination of commercial and residential applications and as such provides an opportunity to investigate the challenges of combining these sources in a single DC microgrid system. The

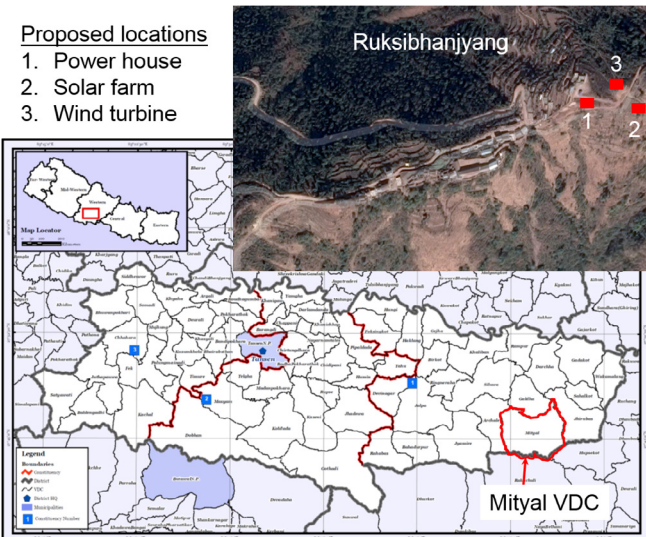


Fig. 3. Ruksibhanjyang, Mityal VDC, Palpa, Nepal (Map [28], Satellite Imagery [29]).

community aim is generate their own power locally through renewable sources, so they can control the cost of the system, and will not be subject to the fuel supply chain which is often disrupted.

The most pertinent local site details for Ruksibhanjyang village are set out in Table 1. The field study assessed both the existing and potential expansion of off-grid supply sources, and provided background information to assist in assessing the future demand and installation requirements for a microgrid in this area. Specifically, the predictions of local energy needs are based on data and local population questionnaires and local resource (wind) data collected locally by PEEDA over the course of several months. The population numbers are based on headcounts carried out in Ruksibhanjyang village. The energy requirements reflect those domestic and economic activities currently carried out by the case study community plus those would be carried out if their energy needs were met. In its site report [26] PEEDA has recommended the installation of a hybrid wind and solar system (Table 1) with a similar percentage mix of sources similar to the successful microgrid installation in December 2011 in Dhaubadi village in the Nawalparasi district of Nepal. In Dhaubadi, two 5 kW wind turbines together with 2 kW of solar power were installed to meet the village's electricity demand of 43.6 kWh per day [26]. PEEDA have recommended a slightly larger renewable installation in the case of Ruksibhanjyang.

PEEDA's study of Ruksibhanjyang was conducted in 2016, the only renewable energy supply was a solar power system installed on the school and connected to 54 surrounding households. It should be noted that no specific storage system or size was recommended as part of PEEDA's field study, but appropriate storage will be required to match the demand throughout the day, which is investigated further in Section 4.

#### 3.2. Modelling demand over 24 h

The field study has provided estimates of the composite domestic, commercial and municipal energy demand per day (Table 1). However, the instantaneous power demand will follow an irregular pattern over the course of a day.

##### 3.2.1. Domestic instantaneous power demand

Fig. 4 shows a rural domestic consumption pattern over a 24-h period in October, based on measured data from Bhanbhane, Gulmi, Nepal in 2012 [30]. As it exhibits typical Nepalese rural domestic consumption patterns over a day, it has been adapted for use in modelling the rural load considered in this work. The measured power over the course of a day on one household in Bhanbhane gave rise to a total energy consumption of 0.39 kWh; this has been normalised to 1 kWh energy consumption over the course of 24 h as shown in Fig. 4. It can then be scaled to reflect the domestic energy demands set out in Table 1.

##### 3.2.2. Commercial and municipal power demand

The commercial and municipal power consumption is more predictable than domestic over the course of 24 h and is shown in Fig. 5. The commercial load is comprised of a water pump, rice mill, and office requirements (photocopy machine and printer). The municipal load comprises office lighting and equipment requirements for a health post, police station, co-operative, VDC office and forestry office.

The separate and combined commercial and municipal power load over the course of 24 h is also shown in Fig. 5.

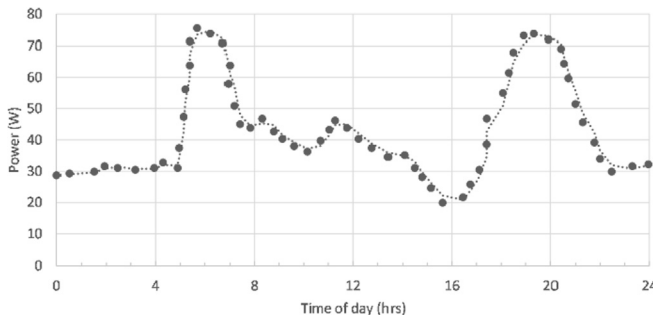
#### 3.3. Modelling solar power

The solar panel modelling technique used is taken from Ref. [31],

**Table 1**

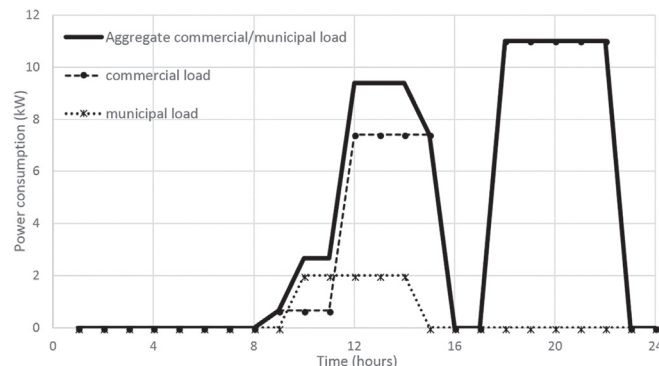
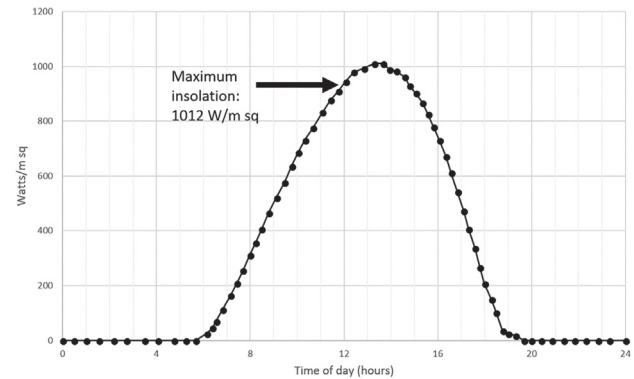
Summary of information from field study site in Nepal.

	Value
Site name	Ruksibhanjyang, Mityal VDC, Palpa, Nepal
Co-ordinates	27°46' N 83°55'E
Elevation above sea level	957 m
No. of households (population)	54 (300)
Available renewable energy sources	Solar, wind
Currently installed renewable power	Average Solar Home System 39 W (min 10 W, max. 180 W), 2.4 kW solar system on school
Currently installed non-renewable power	Commercial - Rice mill diesel engine 7.4 kW
Domestic power demand (daily average)	Domestic – wood, liquid petroleum gas (LPG)
Domestic energy demand per day	6.61 kW average (summer), 3.91 kW (winter)
Current total commercial energy demand per day	58.53 kWh (summer), 30.05 kWh (winter)
Current municipal services demand	86.6 kW (rice mill, water pump, office equipment)
New renewable installations recommended by PEEA to meet current demand following initial site study	2 kW for health posts, police station Three 5 kW wind turbines (total 15 kW), solar panels to aggregate of 5 kW solar

**Fig. 4.** Measured rural domestic power consumption pattern in Nepal over 24-h period (normalised to 1 kWh).

with the photovoltaic panels assumed to be Solarland photovoltaic panels [32], which are currently available in Nepal. The pertinent details for the typical panels are set out in Table 2, which shows they operate with consistent open circuit and rated voltages, with only the rated output current varying as the power output increases.

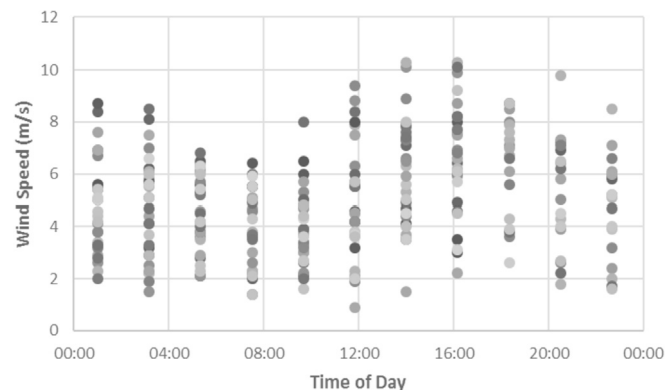
Using site GPS co-ordinates, daily averaged solar data from NASA [33] is used. The site provides an average insolation energy of 5.22 kWh/m<sup>2</sup>/day over the course of a year, increasing in June to 5.8 kWh/m<sup>2</sup>/day. Assuming no cloud cover or shading, the insolation power varies diurnally [34], shown in Fig. 7, reaching a maximum of 1012 W/m<sup>2</sup>. This is then used as an input to the solar panel models for analysis over the course of a day.

**Fig. 5.** Commercial and municipal power consumption requirements in Mityal over 24 h.**Fig. 6.** Diurnal cycle of insolation at Mityal (27° latitude) in June.**Table 2**

Solarland photovoltaic panel details [32].

PV Panel Property	Properties			
STC Rating	20 W	70 W	90 W	140 W
Voltage @ Pmax (Vmp)	17.2 V	17.2 V	17.2 V	17.2 V
Open Circuit Voltage (Voc)	21.6 V	21.6 V	21.6 V	21.6 V
Current at Pmax (Imp)	1.16 A	4.07 A	5.23 A	8.14 A

Photovoltaic panel performance is also temperature dependent, and therefore temperature is an input for the solar panel model. There is no locally recorded temperature information, so an average temperature based on the site location [35] has been used, which is 28.1 °C in June.

**Fig. 7.** Wind speeds measured by AEPC at Ruksibhanjyang.

### 3.4. Modelling wind power

Wind data was recorded at the site every 10 min, and averaged every 2 h, over a period of 9 months at 20, 30 and 40 m by the Alternative Energy Promotion Centre (APEC), Nepal [26], as shown in Fig. 8. This averaged wind speed data is combined with gust modelling, using a small Gaussian distributed random signal with a mean of 0 m/s and a variance of 3 m/s, to determine the wind speed. The wind turbine model used in the Simulink simulation is a 1.5 kW turbine model typical of community scale wind turbines in Nepal and used by the authors in previous work [36].

### 3.5. System layout

From the details given in Ref. [26], the Ruksibhanjyang DC microgrid system layout is shown in Fig. 9.

During the initial field study, suitable solar power, wind turbine and powerhouse locations were identified, as shown in Fig. 3. The distance between the wind turbine and solar panel and the power house, where the solar and wind resource connection points are, is estimated to be 28.3 m and 14.2 m respectively. It is assumed that the storage is located at the powerhouse site. The approximate distance of the transmission line running between the power house site and the village captured during the field visit and was measured to be 1.4 km. Within Ruksibhanjyang village the total distribution wire length was measured to be 1 km. For simplicity, the composite village demand has been modelled as two separate loads, each with cabling to them of 0.5 km. The transmission and distribution distances are illustrated as resistances in Fig. 8. Using standard 100 mm<sup>2</sup> Aluminium Conductor Steel Reinforced (ACSR) lines have been selected for the transmission and distribution lines [26], which will have a resistance of 0.30 Ω/km [37] this gives the line resistance values in Table 3.

### 3.6. Droop control parameters

The droop curves shown in Fig. 3 are used in this simulation, with  $V_{\text{nom}} = 420 \text{ V}$  and  $V_{\text{rated}} = 400 \text{ V}$ . The maximum current,  $I_{\text{rated}}$  is dependent on the power available to the source, or the state of charge of the storage system, and is scaled as described in Section 2 and [25].

The maximum output power from solar panels is approximately proportional to the product of their power rating and insolation, ignoring temperature effects and will therefore vary. Accordingly, the maximum power available from the solar panel, based on the rated panel power at standard conditions and the insolation, is fed forward into the droop controller. This sets the value of the maximum current  $I_{\text{rated}}$  for droop control at minimum voltage

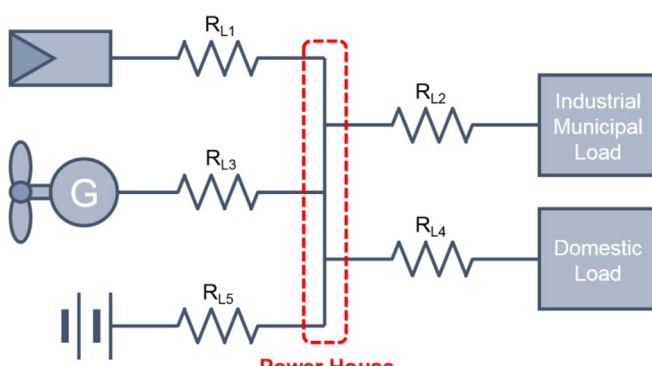


Fig. 8. Ruksibhanjyang DC microgrid layout.

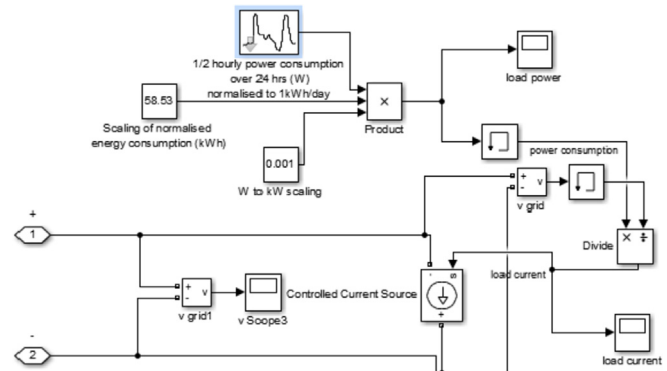


Fig. 9. Simulating 24-h domestic load with scaled variable power consumption in Simulink using a voltage controlled current source.

$V_{\text{rated}}$ .

For the wind turbine, the output power is directly proportional to the cube of the wind speed. As the rated power of the wind turbine at rated speed of 10 m/s is 15 kW, the droop control permits the output voltage to range from its nominal 420 V down to a minimum of 400 V at full output power. Therefore,  $I_{\text{rated}}$  for the wind turbine droop control is 39.47 A at 10 m/s wind speed.

Two different model types have been developed in this work. Section 4 models the system electrical parameters and demonstrates droop control over a short term basis of up to 24 h using Matlab and Simulink. Section 5 investigates system capacity over the course of a year using HOMER.

## 4. Electrical parameters and droop control simulation results

In order to assess the electrical parameters of the system and the efficacy of DC droop control in light of variations over time in solar, wind and loads over the course of a 24 h period, power systems modelling must be carried out. This has been done in Matlab/Simulink as explained in the following sections.

### 4.1. Creation of the DC microgrid model in Simulink

A summary of the key model parameters are shown in Table 4.

The scaled profile varying domestic demand over the course of a day, shown in Fig. 4 was used as an input to the load model in Simulink. Based on a given power consumption profile and measured grid voltage, a signal could be generated to control a controlled current source emulating a load, as shown in Fig. 9.

The composite municipal and industrial load is modelled in Simulink as a second load using the same technique as the domestic load.

The following sections will demonstrate the operation of the linear and non-linear adaptive droop control described in Section 2, then simulate different microgrid arrangements without and with storage.

### 4.2. Adaptive droop control demonstration

To demonstrate the source-power adaptive droop control, a simple simulation is conducted, using a DC source with variable input power that utilises both the linear and non-linear adaptive droop control described in Section 2. With a single source, and droop control parameters previously given in Section 3.6, the load current is varied between 20 and 40 amps, and at 2 s, the maximum output power for the source reduces by half. The source output voltage and current are shown in Fig. 10.

**Table 3**

Line resistance values in DC microgrid.

Line Number	Linking Locations	Distance (m)	Resistance (mΩ)
1	Solar PV – Powerhouse	28	8
2	Powerhouse – Industrial/Municipal Load	1900	570
3	Wind Turbine – Powerhouse	14	4
4	Powerhouse – Domestic Load	1900	570
5	Storage – Powerhouse	0	0

**Table 4**

Summary of power sources, loads and DC network simulation parameters.

Simulated Network Characteristics	Details
Wind turbine	15 kW rated
25 × 200 W solar panels	Aggregate solar power 5 kW
DC distributed network	400 V rated ± 5% at source
System voltage drop	≤10%
Domestic load (Max. Demand)	58.5 kWh in 1 day (4.3 kW)
Commercial load (Max. Demand)	86.6 kWh in 1 day (11 kW)
Municipal load (Max. Demand)	12.0 kWh in 1 day (2 kW)

Fig. 10 shows that as the current demand increases from 20 to 40 A, the voltage in the linear control droops from 416 V to 412 V, whereas the voltage in the non-linear control droops from 419.2 V to 416.8 V. Then, as the source output power drops by half after 1 s, both the linear and non-linear controlled source voltage droops further to 404 V. Finally, when the current demand reduces to 20 A, the linear controlled voltage increases to 412 V, whilst the non-linear controlled version increases to 413 V.

From this, we can see that the non-linear droop control is able to better regulate the output source voltage at the nominal grid voltage, drooping less than the linear control, especially at low voltages. This reduces the need to trade-off power sharing and voltage regulation in this system. This simulation has therefore demonstrated that the droop control is able to change the source output voltage dependent on measured output current and source power.

#### 4.3. DC microgrid with storage

A DC microgrid simulation is created to replicate Ruksibhanjyang's layout, with the generation and load sources described in Section 3, using the linear and non-linear droop control demonstrated in Section 4.2 above. The simulation is run using the residential and combined industrial and municipal loads Figs. 4 and 5, assuming insolation and wind speed from Figs. 6 and 7. It is assumed that the storage can output a maximum aggregate current of 100 A at 400 V, through a power electronic interface. Fig. 11 (a) shows the variation of supply and load currents and voltages over a 24 h period, with Fig. 11 (b) showing the change in battery charge

over the same period using linear droop control. Similar results are obtained for non-linear control.

Fig. 11 shows that at the beginning of the day, there is an excess in generation so the storage in the system will charge, hence the negative current in the battery. As the load increases at 5.30 a.m., the PV and wind generation is not enough to support the load, therefore the battery feeds power into the grid, exporting current into the grid. As the load changes throughout the day, the battery charges and discharges. At the end of the 24 h period, the battery is approximately 80% charged, assuming the system started at 100%. Therefore, the generation is not able to completely support the load, and will require additional generation capacity.

Therefore, we have demonstrated that both linear and non-linear droop control can operate to allow DC sources to supply varying loads under varying source conditions across a day. However, the initial generation source capacity is inadequate to support the time varying load. The insolation, wind speed and load will change over time, whether seasonally or as electrical usage increases over time; therefore a more detailed analysis is required to design the most appropriate size of generation sources and storage capacity to supply the load.

#### 5. HOMER analysis and optimisation of system capacity

The HOMER model is useful in specifying the system capacity requirements for different system permutations for input parameters such as a wind and solar data and demand profiles.

To assess the ability of the proposed renewable energy installation to meet combined domestic municipal and commercial loads in Ruksibhanjyang, Mityal VDC, the source, storage and load requirements have been modelled over the course of one year using HOMER [38] microgrid design software in order to assess the minimum system capacity to meet the village's load requirements.

#### 5.1. Wind power modelling in HOMER

To model the 5 kW wind turbines specified for future installation (Table 1); a generic wind turbine model was used, rather than modelling one from a specific manufacturer. Within HOMER's optimisation parameters, 5 kW DC wind turbine models were

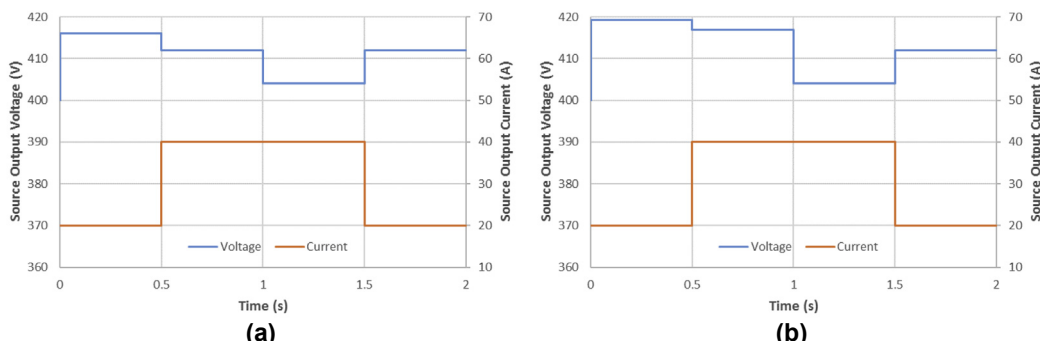
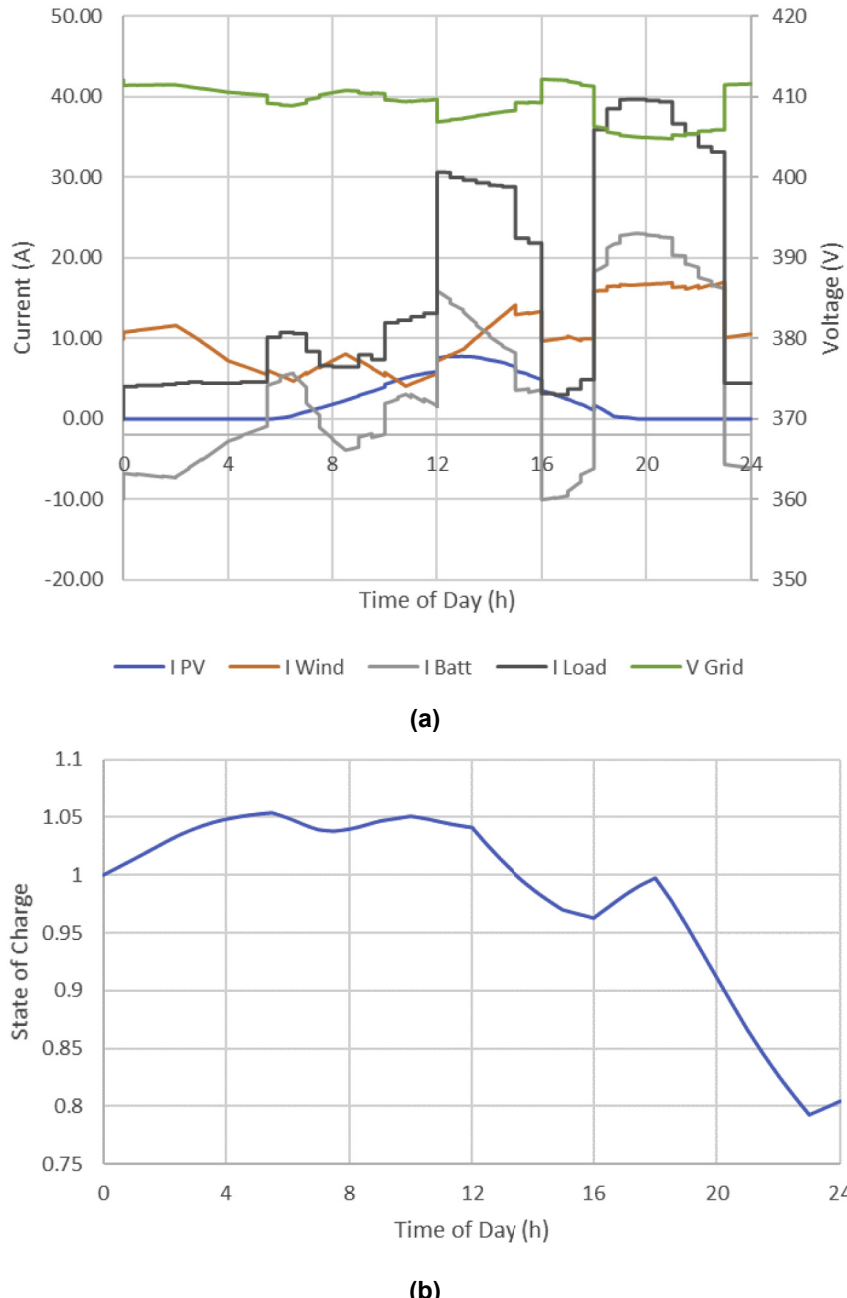


Fig. 10. (a) Linear and (b) Non-linear adaptive droop control demonstration with changing load demand and source maximum output current.



**Fig. 11.** (a) DC microgrid simulation outputs for voltage and current using linear droop control over a 24 h period. (b) Battery state of charge change over a 24 h period. (PV/Wind/Batt – from PV, wind turbine or battery, Load – total load values, I – current, Vgrid – grid voltage at power house).

chosen. The power curve of the turbine, assuming a fixed pitch, stall regulated system, is shown in Fig. 12.

Average monthly wind inputs were used in the HOMER model. These were based on taking an average of the hourly wind measurements at the height of 20 m shown in Fig. 7 set out in the PEEDA site report [26] and is shown in Fig. 13.

## 5.2. Solar power modelling in HOMER

The solar input data for the purposes of modelling in HOMER was provided based on in-built NASA models based on the location and altitude of Ruksibhanjyang specified in Table 1 is shown in Fig. 14.

## 5.3. Load modelling in HOMER

Two separate loads have been modelled in HOMER; a domestic load and a combined municipal/commercial load. In HOMER, the domestic load has been modelled to be the same every day all year round, using the load figures for summer from Table 1 rather than winter to provide a ‘worst case’ analysis. The domestic load modelled on an hourly basis in HOMER is shown as a bar graph in Fig. 15 and is based on a scaled profile shown in Fig. 4.

The hourly combined municipal and commercial load was modelled in HOMER as shown in Fig. 16 which is based on Fig. 5. The combined commercial and municipal load is assumed constant day to day throughout the year.

State of charge of battery at the end of day should be equal or somewhat near what it was at the start of day otherwise the difference in just one day is 20% this means in just a week it would not have any SOC left in it if it is not recharged to near full at the EOD. So a higher Power generation is needed to maintain a Stable system.

Seeing 11(a) it shows that battery current at EOD is same as what it was at the start So either Fig 11(a) is right and Fig 11(b) is wrong or there is some mistake in data.

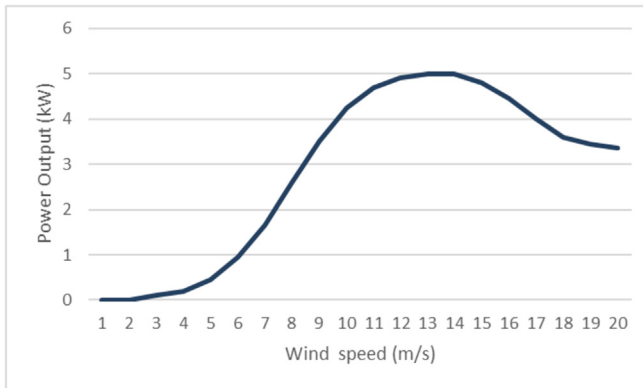


Fig. 12. Power curve for a generic 5 kW wind turbine used in the HOMER model.

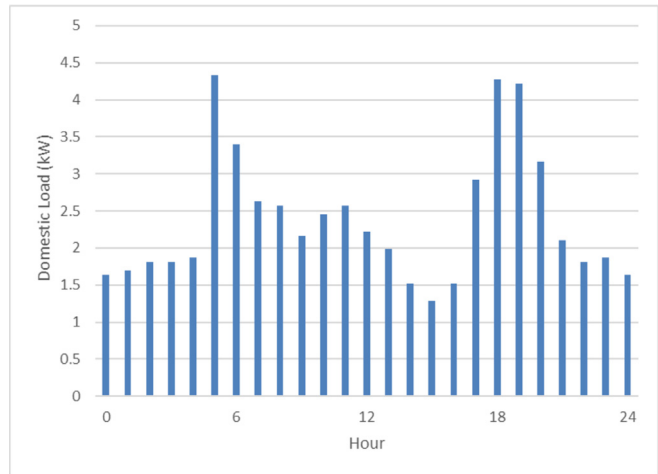


Fig. 15. Daily total domestic load over a year for Ruksibhanjyang based on worst case summer load requirements from Table 1.

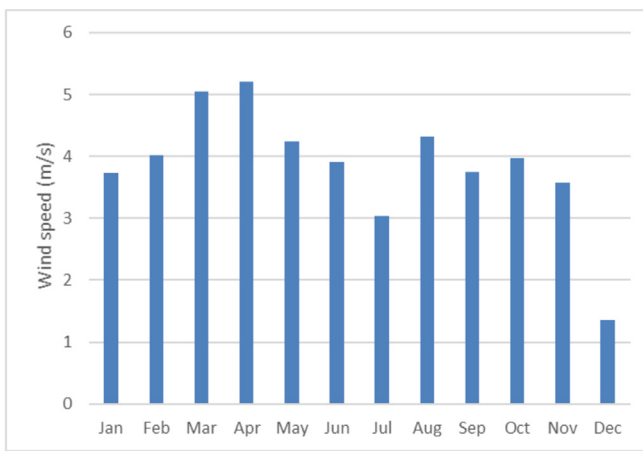


Fig. 13. Average monthly wind input to HOMER model based on hourly measurements taken by APEC in Ruksibhanjyang at a height of 20 m.

#### 5.4. Storage modelling in HOMER

The sizing of battery storage has not explicitly been specified in the PEEA [26] study for the Ruksibhanjyang site. However, for the purposes of modelling in HOMER, strings of **34 Vision CP12240D 12 V batteries** have been chosen to provide storage at a nominal 408 V DC to reflect the specified bus voltage. The capacity of these batteries is each 0.288 kWh and they will thus provide 9.792 kWh of energy storage per string. Assuming the composite domestic,

commercial and municipal energy requirement is approximately 145 kWh per day; this is equivalent to the energy stored in 15 strings each of 34 batteries in length (510 batteries).

#### 5.5. Capacity of PEEA installation recommendations to meet annual energy demand

The initial PEEA site study [26], based on estimated total daily energy requirements for Ruksibhanjyang, recommended that 5 kW solar and 15 kW of wind capacity be installed in the village to meet annual demand.

The HOMER model has initially been set up to verify whether the recommended 5 kW solar and 15 kW wind capacity suggested in the PEEA report was capable of providing the full required capacity over the course of a year, when combined with various storage capacity options during the optimisation. The PEEA report's initial assumptions on power produced by sources and consumed by loads is set out in Table 1.

Running the HOMER model for the search space for 5 kW solar, 15 kW wind and incrementally larger storage capacity resulted in an optimal result within those constraints of a shortfall in annual capacity of 44%. This optimal result with a 44% shortfall requires the

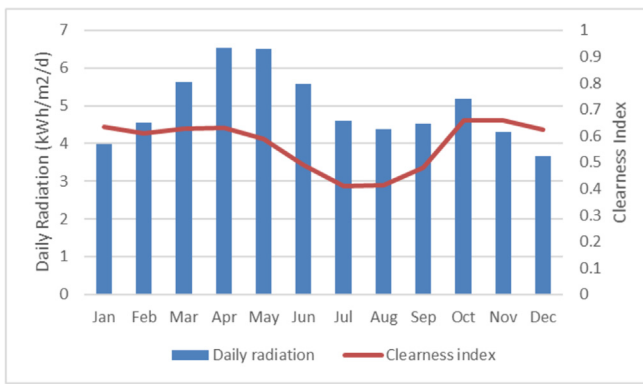


Fig. 14. Solar data from NASA employed in HOMER model based on location and altitude data for Ruksibhanjyang set out in Table 1.

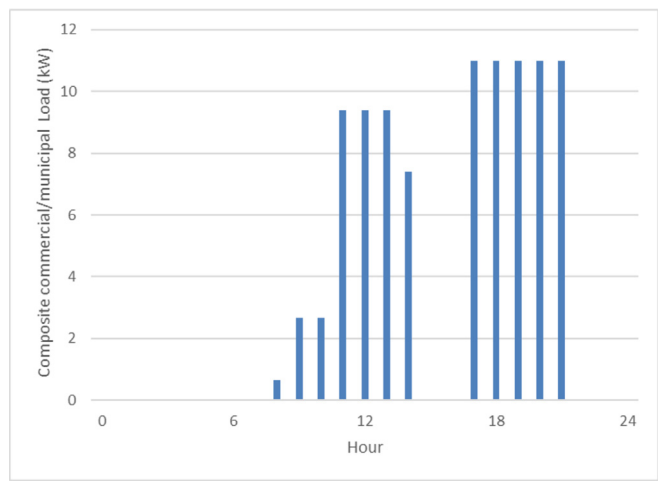


Fig. 16. Daily combined commercial and municipal load over a year for Ruksibhanjyang based on site data [26] set out in Table 1.

installation of 4080 batteries (8 days' worth of storage). Increasing the storage beyond this did not improve the shortfall in capacity.

The shortfall in capacity identified in HOMER arises for several reasons. First, the HOMER model assumes that 100% of Ruksibhanjyang's energy requirement will be met using renewable sources and that the currently installed 7.4 kW rice mill diesel engine referred to in Table 1 will be replaced by renewable power. Second, the PEEDA report compiled initially did not consider the typical daily profile of loads shown in Figs. 16 and 17, but estimated total daily energy requirements. Third, the domestic load modelled in HOMER has been taken to be the higher summer load requirement in order to produce a more conservative model; PEEDA's modelling

assumed a reduction in domestic energy consumption in winter (see Table 1).

##### 5.6. Combinations of solar, wind and storage which collectively meet demand over the course of a year

The HOMER model was therefore adapted to increase the available wind and solar to combinations greater than those recommended by PEEDA [26]. This was to find the minimum combination of wind, solar and storage which will meet Ruksibhanjyan's minimum annual energy requirements. The possible minimum combinations of solar, wind and storage which meet the total

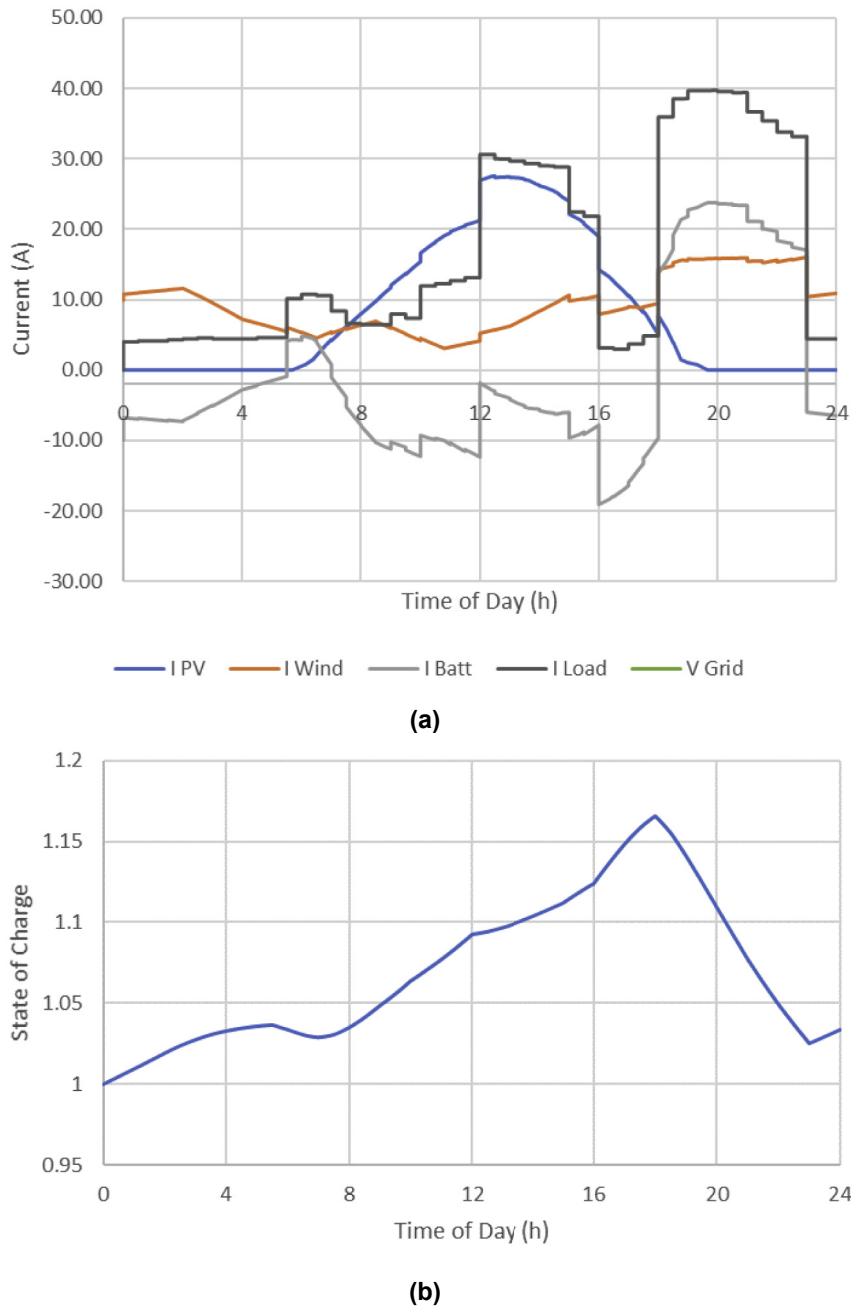


**Fig. 17.** (a) Current measurements from simulation of proposed RuksiBhanjyang DC microgrid with generation able to support year-round load. (b) Normalised battery state-of-charge variation over an example 24 h period.  
(PV/Wind/Batt – from PV, wind turbine or battery, Load – total load values, I – current).

**Table 5**

Minimum energy source and storage combinations to meet required energy capacity over the course of a year.

Resource Type	Viable Combinations providing minimum capacity					
Wind (5 kW turbines)	3	6	3	3	4	3
Solar (kW)	25	20	20	23	21	21
CP12240D 12 V Battery (number)	1020	1020	1530	850	850	1020
Battery storage capacity (kWh)	293.76	293.76	440.64	244.8	244.8	293.76

energy requirements of Rukhsibhanjyang over the course of a year are shown in Table 5. As part of this work, analysis has not been carried out of the relative financial costs of these options in terms of initial installation, ongoing maintenance and replacement costs. As a result, six viable options which meet capacity requirements are presented.

## 6. Discussion

Using the results from the HOMER analysis in Table 5, a further simulation can be run in Simulink to show the first potential solution of generation sources, 15 kW of wind turbines, 25 kWp of solar PV panels and 294 kWh of battery storage. The current measurements from the simulation are shown in Fig. 17 (a), with the battery state of charge shown in Fig. 17 (b).

As can be seen from Fig. 17, the generation sources can still supply the load, with the battery able to recharge itself during the day to return to its original state of charge. With the 5-fold increase in PV generation capacity, this is able to provide more power during the daytime, allowing the battery to charge during the day, before it discharges during the evening demand peaks. There is also sufficient headroom for the system, to allow for load growth.

This microgrid system also demonstrates the expandable, incrementally affordable nature that can be achieved through microgrids. As the load grows, additional generation and storage elements can be added to the system, which is made easier by utilising a distributed control system such as droop control as it requires no knowledge of the system layout, only local measurements of current and voltage. Therefore, if the cost for the required generation or storage to support the full load is not initially available, an initial system can be installed with part-load capacity, and tighter load controls to ensure the microgrid is not overloaded. Then, after some time when additional capital is available, which could potentially be generated from supplying loads from the microgrid system, the full-load capacity of the system can be installed.

## 7. Conclusions

This paper has presented a DC microgrid system, interfacing renewable sources using a power electronic interface with droop functions. A case study site in Rukhsibhanjyang village, Mityal, Nepal is simulated to demonstrate the performance of the system to variable generation and loads. HOMER is used to examine the storage requirements for the insolation, wind and load profiles at Rukhsibhanjyang, Mityal for different combinations of solar and wind generating capacities, showing that the solar and wind system capacity needs to be scaled-up from the initial estimates from PEEDA based on daily energy consumption, to meet the year-round power requirements.

Although numerous previous studies have investigated the use of HOMER and similar software for initial design sizing of hybrid renewable energy systems, the novel aspect of this study is the application of subsequent Simulink analyses to illustrate autonomous power sharing between the specified wind and solar sources. This sharing has been carried out through droop control (adapted

I highly doubt the correctness  
of last three combinations

to include elements which act as a source or sink) and operates in response to changing parameters over the course of a day such as loads and insolation. Storage is included in the daily simulation, demonstrating the benefit of storage in the system, but the requirements of adequate generation to ensure the daily draw on the battery does not exceed the recharging capabilities. Recommendations for further work include developing a hardware in the loop test facility to further investigate system sizing and grid control issues and demand side management. The socio-economic aspects of provision of a new grid have not been examined, therefore appropriate future work would be the examination of socio-economic delivery mechanisms for expandable microgrid technologies and exploring the economic pay-off between generation and storage capacity costs.

## Acknowledgements

The funding of this research has been provided by a UK EPSRC Global Challenges Project Institutional Sponsorship Grant.

## References

- [1] International Energy Agency. "World energy outlook", organisation for economic Co-operation and development. 2016. London.
- [2] United Nations, "UN sustainable development goals", Available from: <https://sustainabledevelopment.un.org/>.
- [3] Guerrero JM. Hierarchical control of droop-controlled AC and DC microgrids 2014; A General Approach Toward Standardization. IEEE Trans Ind Electron 2011;58:158–72.
- [4] Choi J, Jeong H, Choi J, Won D, Ahn S, Moon S. Voltage control scheme with distributed generation and grid connected converter in a DC microgrid. Energies 2014;7:6477–91.
- [5] Los Alamos National Laboratory. DC microgrids scoping study—estimate of technical and economic benefits. 2015. Los Alamos.
- [6] Vasquez JC, Mastromarco RA, Guerrero JM, Liserre M. "Voltage support provided by a droop-controlled multifunctional inverter". IEEE Trans Ind Electron 2009;56:4510–9.
- [7] Prinsloo G, Mammoli A, Dobson R. Customer domain supply and load coordination: a case for smart villages and transactive control in rural off-grid microgrids. Energy 2017;135:430–41.
- [8] Sinha S, Chandel SS. Review of software tools for hybrid renewable energy systems. Renew Sustain Energy Rev 2014;32:192–205.
- [9] Kasara BU, Parekh BR. Modelling and simulation of distributed generation system using HOMER software. In: Proc. Int. Conf. Recent advancements in electrical, electronics and control engineering, Sivakasi; 2011.
- [10] R. Sen, S. C. Bhattacharyya, "Off-grid electricity generation with renewable energy technologies in India: an application of HOMER", Renew Energy, vol. 62, pp. 388–398.
- [11] Nazir R, Laksono HD, Waldi EP, Ekaputra E, Coveria P. Renewable energy sources optimization: a micro-grid model design. Energy Procedia 2014;52: 316–27.
- [12] Quiggin D, Cornell S, Tierney M, Buswell R. A simulation and optimisation study: towards a decentralised microgrid, using real world fluctuation data. Energy 2012;41:549–59.
- [13] Luna AC, Diaz NL, Graells M, Vasquez JC, Guerrero JM. "Mixed-Integer-Linear-Programming-Based energy management system for hybrid PV-wind-battery microgrids: modeling, design, and experimental verification. IEEE Trans Power Electron 2017;32:2769–83.
- [14] Yu K, Ai Q, Wang S, Ni J, Lv T. Analysis and optimization of droop controller for microgrid system based on small-signal dynamic model. IEEE Trans Smart Grid 2016;7:695–705.
- [15] Lopes JAP, Moreira CL, Madureira AG. Defining control strategies for Micro-Grids islanded operation. IEEE Trans Power Syst 2006;21:916–24.
- [16] Ou TC, Hong CM. Dynamic operation and control of microgrid hybrid power systems. Energy 2014;66:314–23.
- [17] Panda A, Choudhury S, Chatterjee D. Microgrid based hybrid energy Co-

- operative for grid-isolated remote rural village power supply for east coast zone of India. *IEEE Trans Sustain Energy* 2018;9:1375–83.
- [18] Banerjee P, Pandey K, Mathur D. Designing and simulation of standalone micro grid for rural area using renewable energy resources. In: Proc. India international conference on power electronics, Patiala; 2016.
- [19] Al-Falahi MDA, et al. Sizing and modeling of a standalone hybrid renewable energy system. In: Proc. IEEE annual southern power electronics conference, Auckland; 2016.
- [20] Justo JJ, Mwasilu F, Lee J, Jung J. AC-microgrids versus DC-microgrids with distributed energy resources: a review. *Renew Sustain Energy Rev* 2013;24: 387–405.
- [21] Nehrir MH, Wang C, Strunz K, Aki H, Ramakumar R, Bing J, Miao Z, Salameh Z. A review of hybrid renewable/alternative energy systems for electric power generation: configurations, control, and applications. *IEEE Trans Sustain Energy* 2011;2:392–403.
- [22] Kablac E. An islanded hybrid microgrid design with decentralized DC and AC subgrid controllers. *Energy* 2018;153:185–99.
- [23] Asad R, Kazemi A. A novel distributed optimal power sharing method for radial dc microgrids with different distributed energy sources. *Energy* 2014;72:291–9.
- [24] Khorsandi A, Ashourloo M, Mokhtari H. An adaptive droop control method for low voltage DC microgrids. In: Proc. Power Electronics, Drive System, And technologies conference, Tehran; 2014.
- [25] Williamson SJ, Griffio A, Stark BH, Booker JD. A controller for single-phase parallel inverters in a variable head pico-hydropower off-grid network. *Sustain Energy Grids Network* 2016;5:114–24.
- [26] Chand T, Gautam B. PEEDA field study report in mityal, Ruksibhanjyang, Palpa district, Nepal. Kathmandu: People, Energy & Environment Development Association; December 2016.
- [27] PEEDA website – PEEDA's previous projects, Available from: <http://peeda.net/activities/previous-projects> [Accessed 07/05/2018].
- [28] United Nations, Palpa Map, Available from: <http://www.un.org.np/maps/nepal-palpa-district-map-constituency-boundary> [Accessed 07/05/2018].
- [29] Satellite Imagery – Google Maps/CNES/Airbus, Available from: <https://www.google.co.uk/maps/@27.7694666,83.919764,639m/data=!3m1!1e3>, [Accessed 07/05/2018].
- [30] Williamson SJ. Modular and scalable low-head pico-hydro generation for off-grid networks. PhD Thesis. University of Bristol; 2014.
- [31] Kitson J, Williamson SJ, Harper P, McMahon CM, Rosenberg G, Tierney M, Bell K. A photovoltaic panel modelling method for flexible implementation in Matlab/Simulink using datasheet quantities. In: Proc. IEEE international symposium on industrial electronics, Edinburgh; 2017.
- [32] Solarland PV panels, Available from: <https://www.solarlandusa.com/standard.html> [Accessed 07/05/2018].
- [33] National Aeronautics and Space Administration, NASA atmospheric science data center, Available from: <https://eosweb.larc.nasa.gov>, [Accessed 07/05/2018].
- [34] Colorado State University, Sunshine on a perfectly cloudless day, Available from: <http://biocycle.atmos.colostate.edu/shiny/solar/>.
- [35] World Bank, World bank climate change portal – Nepal, Available from: [http://sdwebx.worldbank.org/climateportal/index.cfm?page=country\\_historical\\_climate&ThisCCode=NPL](http://sdwebx.worldbank.org/climateportal/index.cfm?page=country_historical_climate&ThisCCode=NPL) [Accessed 07/05/2018].
- [36] Kishor N, Fraile-Ardanuy J. *Modeling and Dynamic Behaviour of Hydropower Plants*, Chapter 11 (Williamson et al). IET; 2017.
- [37] World Bank. Mini grid design manual. Washington DC: ESMAP; 2000.
- [38] National Renewable Energy Laboratory, HOMER website, Available from: <http://www.homerenergy.com> [Accessed 07/05/2018].